

Numerical studies of the suppression of vortex-induced vibrations of twin box girders by central grids

Zhiguo Li^a, Qiang Zhou^{*}, Haili Liao^b and Cunming Ma^c

Research Center for Wind Engineering, Southwest Jiaotong University, Chengdu, China

(Received September 18, 2017, Revised December 22, 2017, Accepted January 11, 2018)

Abstract. A numerical study based on a delayed detached eddy simulation (DDES) is conducted to investigate the aerodynamic mechanism behind the suppression of vortex-induced vibrations (VIVs) of twin box girders by central grids, which have an inhibition effect on VIVs, as evidenced by the results of section model wind tunnel tests. The mean aerodynamic force coefficients with different attack angles are compared with experimental results to validate the numerical method. Next, the flow structures around the deck and the aerodynamic forces on the deck are analyzed to enhance the understanding of the occurrence of VIVs and the suppression of VIVs by the application of central grids. The results show that shear layers are separated from the upper railings and lower overhauled track of the upstream girder and induce large-scale vortices in the gap that cause periodical lift forces of large amplitude acting on the downstream girder, resulting in VIVs of the bridge deck. However, the VIVs are apparently suppressed by the central grids because the vortices in the central gap are reduced into smaller vortices and become weaker, causing slightly fluctuating lift forces on the deck. In addition, the mean lift force on the deck is mainly caused by the upstream girder, whereas the fluctuating lift force is mainly caused by the downstream girder.

Keywords: twin box girders; vortex-induced vibrations; central grids; CFD simulation

1. Introduction

With the increase in the span length of bridges, wind-induced oscillations, which include galloping, flutter, and vortex-induced vibrations (VIVs), have become an issue of serious concern to modern bridge engineers. The application of two twin box girder sections is one approach for improving aerodynamic stability (Ge and Xiang 2008); examples of this approach are the Xihoumen suspension bridge (main span: 1650 m, China), the Stonecutters cable-stayed bridge (main span: 1018 m, Hongkong), and the Gwangyang suspension bridge (main span: 1545 m, Korea). Recently, a new suspension bridge, named the Lingdingyang Bridge, with two twin box girders and a main span of 1660 m has been planned for construction in south China. Figs. 1 and 2 present the span arrangement and the cross section of the bridge deck, respectively.

Even though it has been reported that the twin box girder configuration exhibits a higher critical flutter wind speed (Ogawa *et al.* 2002, Matsumoto *et al.* 2004, Hui *et al.* 2006, Yang and Ge 2009, Kwok *et al.* 2012, Trein *et al.* 2015), the problem of VIV tends to arise for twin box girders due to the complicated flow around the box and gap

as well as the interference between the two girders. Most of the existing literature regarding the VIV of bridges has focused on a single girder or rectangular deck (e.g., Matsumoto *et al.* 2008, Hua *et al.* 2015, Xu *et al.* 2015, Xu *et al.* 2017). Some attentions have been paid to the VIV of a long span bridge with two box girders. Chen *et al.* (2007) studied the wind-induced vortex shedding of two parallel box-girder bridges using wind tunnel tests; the results showed that the aerodynamic interference cannot be ignored and that it affected the VIV of both decks. Larsen *et al.* (2008) observed the obvious VIV of the Stonecutters bridge, which has a twin box girder section, and investigated experimentally the suppression effect of guide vanes. Li *et al.* (2011) investigated the VIV of a twin steel box girder suspension bridge with a main span of 1650 m based on field measurements and indicated that the VIV more likely occurs in a low wind speed range of 6~10 m/s, with the wind direction nearly perpendicular to the bridge line, and at low turbulence intensity. Chen *et al.* (2014) studied the unsteady vortices and turbulent flow structures around twin box girder bridge deck models with different gap ratios using section model tests. Kargarmoakhar *et al.* (2015) investigated experimentally the effects of the Reynolds number on the aerodynamic characteristics of a twin-deck bridge in the range of $Re=1.3\times 10^6\sim 6.1\times 10^6$; the authors found that a larger separation bubble formed on the bottom surface of the upstream girder, accompanied with a narrower wake region with increasing Re number. Yang *et al.* (2016) conducted a series of wind tunnel tests to investigate the VIV characteristics and countermeasures for twin box girder bridges and mentioned that the application of grid plates has positive effects on suppressing the heaving VIV responses.

*Corresponding author, Ph.D.

E-mail: milan1023@gmail.com

^a Ph.D. Student

E-mail: lizhiguo@swjtu.edu.cn

^b Professor

E-mail: hlliao@swjtu.edu.cn

^c Associate Professor

E-mail: mcm@swjtu.edu.cn

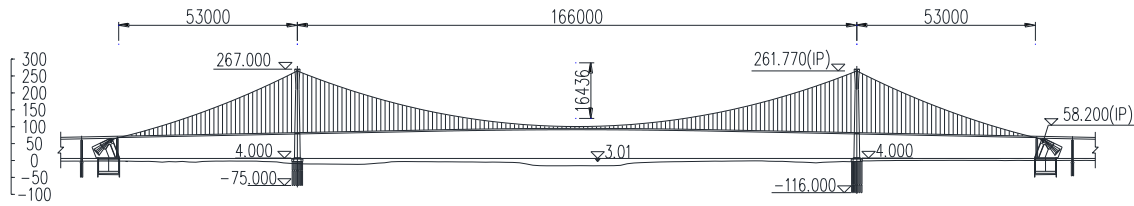


Fig. 1 General layout of the suspension bridge (unit: cm)

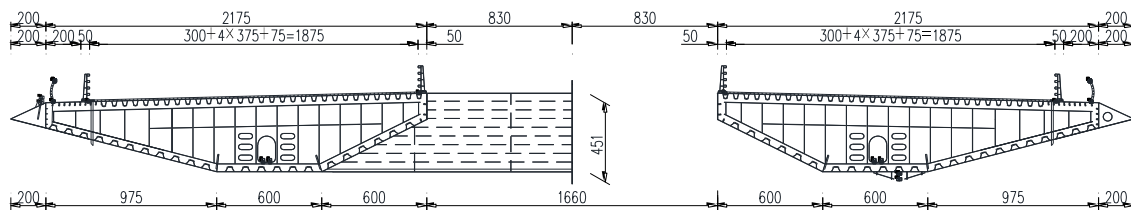


Fig. 2 Cross section of the bridge deck (unit: cm)

Moreover, with the development of computational fluid dynamic (CFD) methods, an increasing number of researchers are investigating the aerodynamic behavior of a bridge deck and the VIV characteristics using a computational approach. Zhou and Ma (2010) applied the deterministic vortex method to perform a computational study of the Reynolds number effect on two bridge decks based on an analysis of the aerodynamic coefficients, Strouhal number, and pressure distribution. Nieto *et al.* (2010) performed a two-dimensional (2D) numerical study to investigate the vortex-shedding response of a twin box deck cable-stayed bridge and obtained reasonable results. Zhou *et al.* (2015) investigated numerically the suppression of different countermeasures for the VIV of a bridge deck with a long projecting slab by applying the SST $k-\omega$ model. de Miranda *et al.* (2015) performed LES and RANS to simulate the flow around four sets of twin box girders with different gap spaces. Their results showed that LES provides better results than RANS. In addition, Sun *et al.* (2008) suggested that the $k-\omega$ performs better than $k-\epsilon$ for wall flow simulation because the latter over-produces turbulent kinetic energy near the wall with changing flow patterns. Thus, it may be more suitable to apply the DDES (delayed detached eddy simulation) with the SST $k-\omega$ model, which is a combination of the LES and RANS of the SST $k-\omega$ model, to simulate flow around the two twin box girders with consideration given to both the accuracy and efficiency.

Based on the above observations, there are many research studies on the VIV performance of twin box girders, and some aerodynamic countermeasures have been proposed to control the VIV. However, less attention has been paid to either the mechanism of VIV or the mechanism of aerodynamic countermeasures. Hence, in the present study, the flow around two box girders is investigated by performing 2D DDES with the SST $k-\omega$ model at Reynolds number $Re=U_\infty D/\nu=2.5\times 10^4$ (the same as that in the wind tunnel tests), where U_∞ is the free stream velocity, D is the thickness of the deck, and ν is the kinematic viscosity. The numerical method and numerical details applied in this

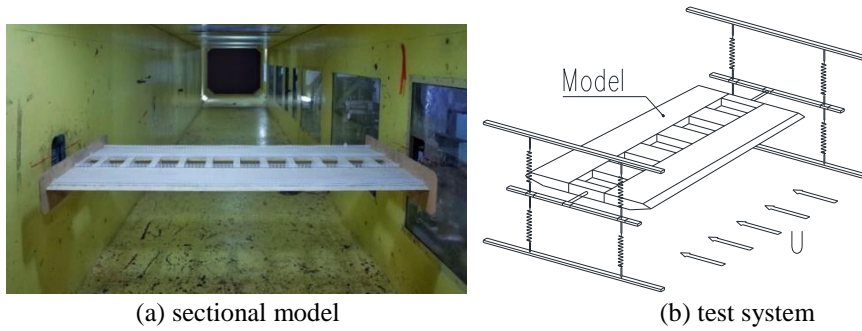
study are first described and verified by presenting the mean aerodynamic coefficients and Strouhal number. Next, we focus on the time-averaged and instantaneous flow structures, pressure distributions, and forces on two girders to study the underlying mechanism of VIV and the suppression of central grids. In addition, the components of the total aerodynamic forces are analyzed.

2. Description of the experiment

In this study, wind tunnel tests were performed to facilitate the comparison between the experimental and numerical results. The experimental study was conducted in a closed-circuit wind tunnel with a test section of 2.4 m height \times 2.0 m width \times 16.0 m length using wind velocities ranging from 1.0 m/s to 45 m/s. A test set-up, which was specially designed to perform static and dynamic tests of bridge deck sections and was mounted on the outside walls of the wind tunnel, was used in the wind tunnel testing.

The dynamic model (1:70) was suspended by four pairs of linear springs to facilitate the vertical and torsional motions of the bridge deck models, as shown in Fig. 3. The dynamic sectional-model tests were conducted under smooth oncoming flow with five attack angles of 0° , $\pm 3^\circ$, and $\pm 5^\circ$.

As shown in Fig. 4, two VIV regions were observed within the reduced wind velocity ranges of 0.07-0.09 and 0.11-0.13, which correspond to the Strouhal numbers derived from the static loading shown in Table 1, and the maximum amplitudes of vertical vibration of prototype twin-box deck (identified as the original deck, also in the following) were 0.34 m and 0.69 m, respectively, which are significantly larger than the requirements of both Chinese and British Codes. Hence, the central grids on the upper side of the gap with different flux ratios were employed to mitigate the VIV, as shown in Fig. 5. Here, the flux ratio is defined as $Flux\ ratio=(n+1)\times b/L$, where n is the number of central grids, and b and L are the spacing between two grids and the gap, respectively. The flux ratios of 0%, 17%, 25%,



(a) sectional model

(b) test system

Fig. 3 Schematic diagram of the model test

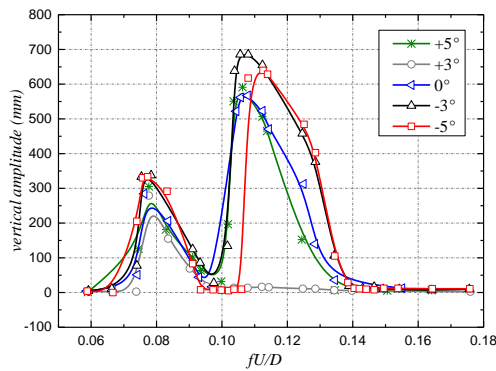
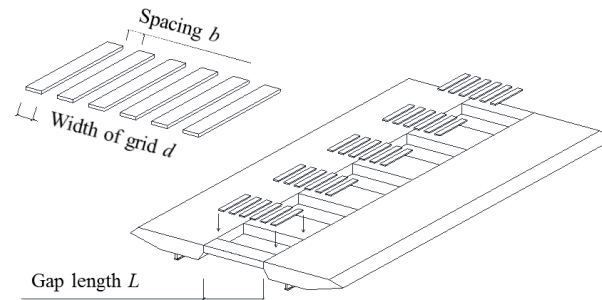


Fig. 4 The responses of the vertical VIV of the original deck



(a) the central grids on the sectional model



(b) schematic diagram of central grids with different flux ratios

Fig. 5 The aerodynamic countermeasures of the central grids

33%, 42%, 50%, 67%, 75%, and 83% were studied in the present study.

As shown in Fig. 6, the VIV was suppressed by placement of the central grids at all studied attack angles. The effects of central grids were also studied in the experimental studies of Yang *et al.* (2016). However, in

contrast to their results, where the effectiveness of the central grids was more pronounced with the decrease of flux ratio, we found that the VIV disappeared when a flux ratio of 50% had been achieved.

Here, the deck with the central grids and a flux ratio of 50%, as shown in Fig. 5(b), was identified as the optimized

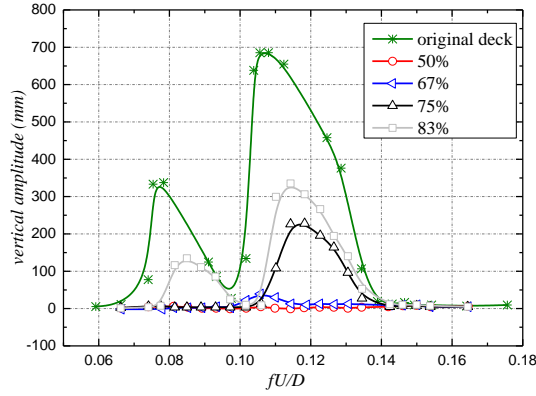


Fig. 6 The vertical VIV of the deck with central grids for the attack angle of -3°

deck (also in the following). To investigate the aerodynamic mechanism on the suppression of VIV of the twin box girders by central grids, the flow around the original and optimized decks was numerically studied for the most unfavorable attack angle of -3° .

3. Numerical setup

3.1 Governing equations

The numerical model for flow around two tandem circular cylinders is formulated using the Cartesian coordinate system. Eqs. (2) and (3) show the filtered continuity and the Navier-Stokes equations, respectively.

$$\frac{\partial \bar{u}_i}{\partial x_i} = 0 \quad (1)$$

$$\frac{\partial (\bar{u}_i)}{\partial t} + \frac{\partial (\bar{u}_i \bar{u}_j)}{\partial x_j} = -\frac{1}{\rho} \frac{\partial \bar{P}}{\partial x_i} + \nu \frac{\partial^2 \bar{u}_i}{\partial x_j \partial x_j} - \frac{\partial \tau_{ij}}{\partial x_j} \quad (2)$$

where u_i ($i=1, 2, 3$) are the three velocity components. ρ , P , and ν represent the air density, pressure, and kinematic viscosity of the flow, respectively. τ_{ij} is the stress, which is used to denote the subgrid scale stresses in the LES model far from the wall, and τ_{ij} is expressed in the SST $k-\omega$ model in the near wall region based on the following function (Spalart *et al.* 1997, Menter *et al.* 2003)

$$F_{DES} = \max \left(\frac{L_t}{C_{DES} \Delta_{\max}}, 1 \right) \quad (3)$$

where $C_{DES} = 0.61$, Δ_{\max} is the maximum grid spacing, and L_t is the turbulence length scale in the SST $k-\omega$ model. However, the DES limiter can activate the LES mode inside the boundary layer, where the grid is not fine enough to sustain resolved turbulence. Therefore, a new

formulation of DES is employed to preserve the RANS mode throughout the boundary layer (Spalart *et al.* 2006). This approach is known as the delayed option, or DDES. The function is modified as follows

$$F_{DES} = \max \left(\frac{L_t}{C_{DES} \Delta_{\max}} (1 - F_{SST}), 1 \right) \quad (4)$$

where F_{SST} is equal to 0, F_1 , or F_2 , which are the blending functions of the SST $k-\omega$ model.

3.2 Numerical discretization and algorithm

The simulation is performed with the aid of the Fluent® package. The simulation options offered by Fluent® can be carefully selected or set by the user definite function (UDF) on the following basis.

In the simulation, the velocity and pressure are defined at the center of a control volume, while the volume fluxes are defined at the midpoint of their corresponding cell surfaces. The momentum interpolation method (MIM) is used to avoid oscillating problems by eliminating the checkerboard pressure and subsequent refinements with a non-staggered mesh. The SIMPLE (semi-implicit method for pressure-linked equations) algorithm proposed by Patankar and Spalding (1972) is utilized. In addition, the convergence criterion of the iterative calculation is set to 1×10^{-6} , which requires approximately 10 iterations to satisfy.

To avoid the instability caused by central-differencing schemes and non-physical wiggles, the bounded central differencing scheme is applied to the spatial differencing of the convection term, which is a composite normalized variable diagram (NVD, (Leonard 1991)) scheme. Moreover, a fully implicit second-order time-advancement scheme is chosen for temporal discretization to obtain a stable and accurate simulation.

3.3 Grid system and boundary conditions

As shown in Fig. 7, the computational domain is $140D$ in the x -direction and $50D$ in the y -direction. The blockage ratio is 2%, which is smaller than the suggestion (6.4%) of Sohankar (2008).

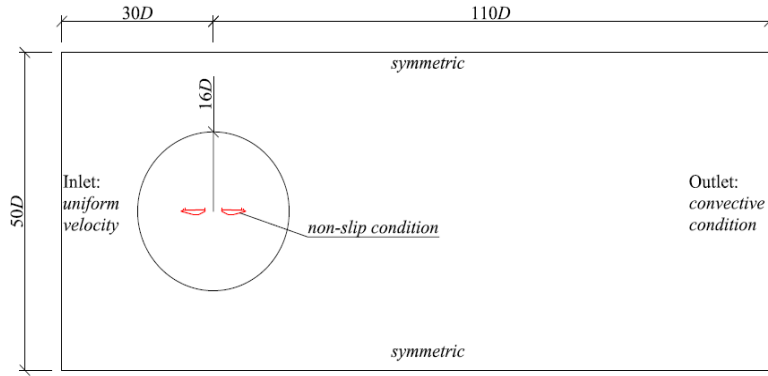


Fig. 7 Computational domain and boundary conditions

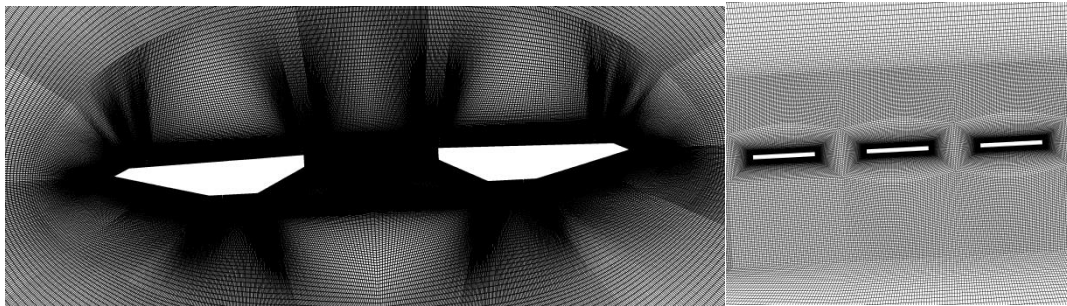


Fig. 8 Close-up view of the grid system

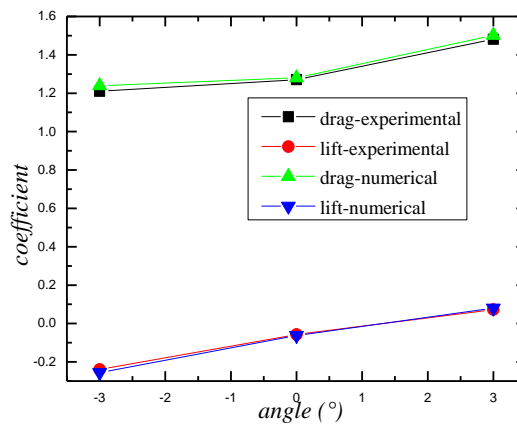


Fig. 9 Comparison of the numerical and experimental aerodynamic coefficients

Fig. 8 presents the grid near the deck and central girders. Structured O-type grid systems with the depth of the first grid near the body surface given empirically as $0.1/Re^{0.5}$ are applied to adequately resolve the flow. For more efficient simulations, the computational domain is spatially resolved such that a dense clustering of grid points is applied near the wall, especially in the wake zone, whereas a coarser grid is used away from the wall. For the temporal discretization, the non-dimensional time-step $\Delta t^* = \Delta t U / D$ (Δt : the time-step for calculation) is 2.5×10^{-3} , which maintains the Courant number less than 1.

The boundary conditions for the simulation, illustrated in Fig. 7, are as follows:

Body surface: A no-slip condition for $u_i=0$ and a Neumann condition for pseudo-pressure ϕ are imposed.

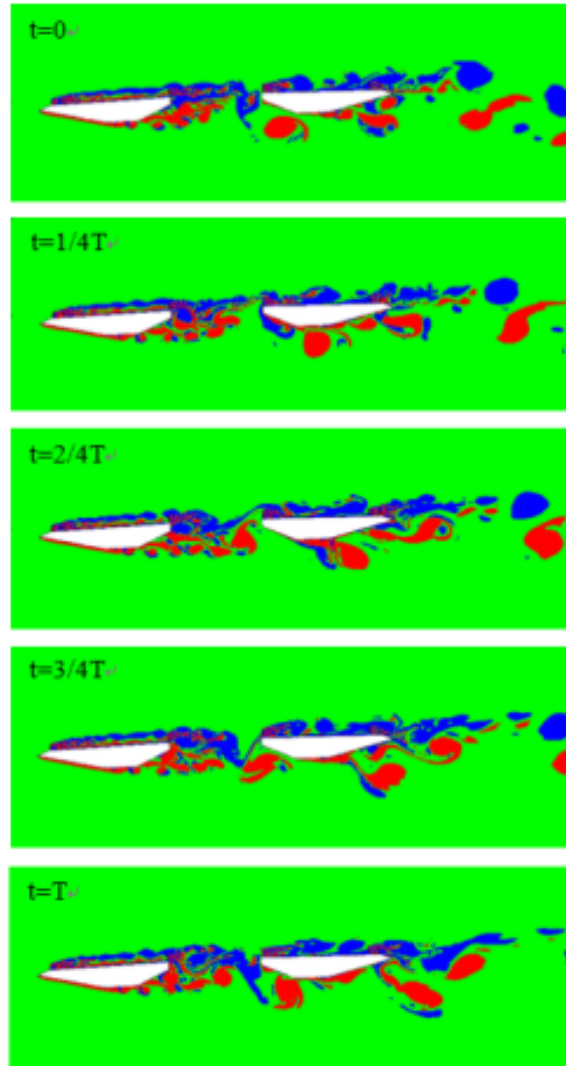
Inlet: The uniform velocity condition, $u=10$ m/s, $v=0$, and $w=0$, and a Neumann condition of pseudo-pressure ϕ are imposed at the inlet boundary.

Outflow boundary: A convective boundary condition ($\partial \phi / \partial t + \bar{u} \cdot \partial \phi / \partial x = 0$) is applied for velocity, and the Neumann condition is applied for pseudo-pressure.

Upper and lower sides: A symmetric condition is applied to both velocity and pseudo-pressure.

Table 1 Comparison of Strouhal numbers

Strouhal number	Experimental result	Numerical result	Difference
vortex-induced region 1	0.081	0.085	4.94%
vortex-induced region 2	0.121	0.130	7.44%

Fig. 10 Instantaneous vorticities around the original deck in one period ($\omega = \pm 1.5$)

3.4 Numerical validation

To validate the present simulation, the aerodynamic coefficients and Strouhal number of the original deck are compared with those of the experimental studies.

As shown in Fig. 9, the aerodynamic coefficients of the original deck with attack angles of 0° and $\pm 3^\circ$ agree well with the experimental data, although the numerical value is slightly larger because of the two-dimensional simulation in this study.

As shown in Table 1, the Strouhal numbers obtained by the present simulation differ by less than 8% relative to those of the experimental result, which suggests that the numerical results are consistent with the experimental

results. Hence, the numerical method and the grid system utilized in the present simulation provide reasonably good simulation results.

4. Results and discussion

4.1 Flow structures

Fig. 10 shows the contours of instantaneous vorticities for the original deck with an attack angle of -3° in one period, where the blue and red colors represent clockwise and counterclockwise vortices, respectively. Similar to the flow pattern of two tandem cylinders named the co-

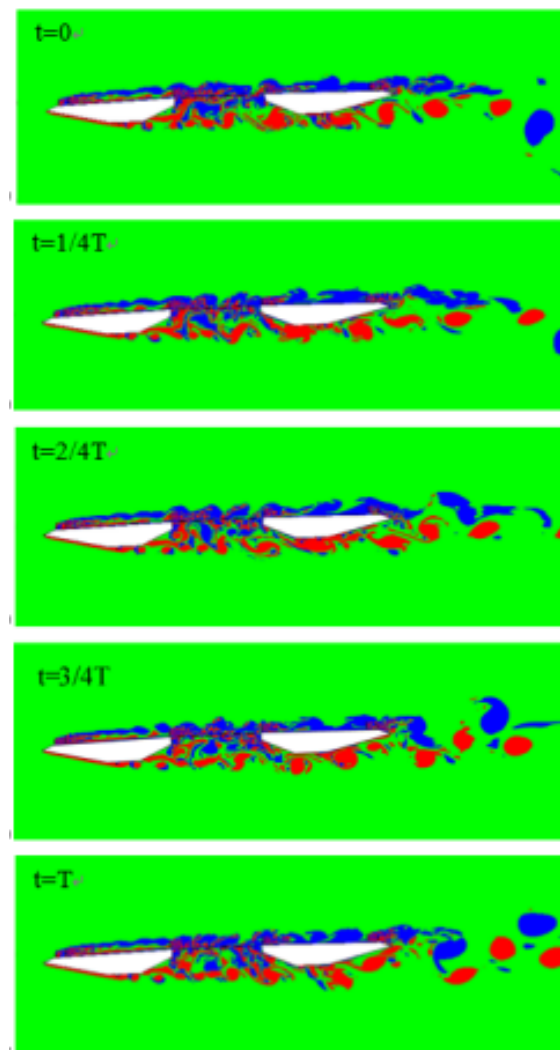


Fig. 11 Instantaneous vorticities around optimized deck in one period ($\omega = \pm 1.5$)

shedding regime (Alam *et al.* 2003), the alternate vortex shedding occur in the gap as well as in the wake of the downstream girder, suggesting that the binary vortex street appears in the wakes. Moreover, it can be found that the shear layers separate from the upper railings and the lower overhaul track of the upstream girder, thereby inducing the large-scale vortices that are formed in the gap. Next, the vortices impinge alternately onto both the upper and lower sides of the downstream girder, i.e., the upper vortices formed by the shear layers separate from the upper railings and the lower vortices formed by the shear layers separate from the lower overhaul track, which would not only affect the upper surface but also the lower surface of the downstream girder. Hence, this flow behavior would induce a larger lift fluctuation and may cause VIVs.

As shown in Fig. 11, the binary vortex street also appears in the case of the optimized deck with the attack angle of -3° . However, it can be observed that the large-scale vortices that appear in the case of the original deck are obviously suppressed and reduced into small-scale vortices after placing central grids in the gap. Moreover, the interaction between the upper and lower vortices is impeded

and becomes weaker. It can also be found that the upper vortices and lower vortices impinge onto the upper and lower surfaces of the downstream girder, respectively. In addition, the width of the movement of the vortices in the gap and the wake of the downstream girder becomes narrower because of the existence of the central grids. This indicates that the aerodynamic forces on the deck are affected by the change of the flow behavior.

Figs. 12 and 13 show the time-averaged streamline around the original deck and the optimized deck, as well as in their gap, for the attack angle of -3° . Regarding the original and the optimized decks, there are two main vortices, one behind the oblique web of the upstream girder (named as the first vortex) and the other in the gap (named as the second vortex); these vortices are formed by the shear layers separated from the upper railings and lower overhaul track of the upstream girder, respectively. Zhou *et al.* (2015) also found a similar phenomenon in their numerical simulations. These results also indicate that the two VIV lock-in regions are induced by these two main vortices. As shown in Fig. 12, the flow that passes over the upper side of the upstream girder has a significant downward velocity at

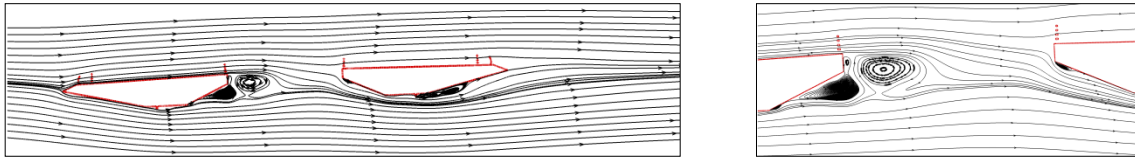


Fig. 12 Time-averaged streamline around the original deck for the attack angle of -3°

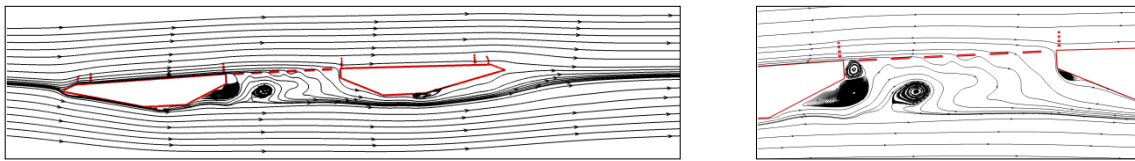
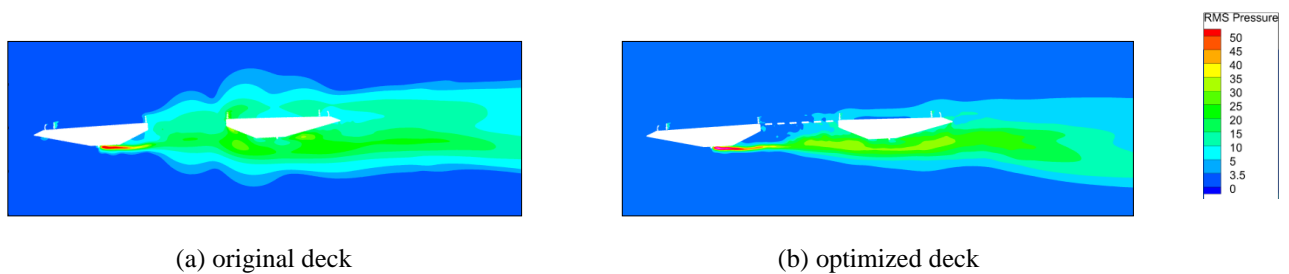


Fig. 13 Time-averaged streamline around the optimized deck for the attack angle of -3°



(a) original deck

(b) optimized deck

Fig. 14 Contours of the fluctuating pressure around the decks

the central gap and impinges onto the bottom of the downstream girder. This result illustrates that interference between the upper and lower vortices is strong and that the large-scale vortices formed by the upstream girder impinge alternately onto the upper and lower surfaces of the downstream girder.

However, after placing central grids in the gap, the second vortex is suppressed to a relatively smaller scale, as shown in Fig. 13. Moreover, the downward flow in the gap is significantly inhibited, which illustrates that the interaction between the upper and lower vortices is obstructed because of the existence of the central grids. The change in the flow structures around the deck affects the forces on the deck, especially the fluctuating forces. In addition, the vortices in the wake of the downstream girder are weaker than those in the wake of the upstream girder, as observed for both cases of the original and optimized decks. This demonstrates that the total mean drag and lift forces on the deck are mainly contributed by the upstream girder, as will be discussed in detail in the following section.

4.2 Aerodynamic forces

To further explain the aerodynamic mechanism that suppresses the VIV of two twin box girders by central grids, the aerodynamic forces associated with the flow behavior around the deck are discussed in this section. Fig. 14 presents the contour of the fluctuating pressure around the

original and optimized decks. This figure shows that the fluctuating pressure distribution of the original deck is more extensive, especially in the central slot and around the downstream girder. Moreover, regarding the original deck, the pressure on the bottom surface of the downstream girder pulsates more strongly, whereas the pressure distribution around the optimized deck shows a weak feature. This phenomenon primarily occurs because the impingement of vortices onto the downstream girder is weakened by the existence of the central grids.

Fig. 15 compares the distributions of fluctuating pressure (root mean square value of the pressure) on the surfaces between the original deck and the optimized deck. The fluctuating pressure on the downstream girder is significantly higher than that on the upstream girder because of the impingement of vortices onto the downstream girder. The upstream girders for both the original deck and the optimized deck show a similar pressure distribution, which suggests that the central grids have little influence on the fluctuating pressure of the upstream girder. However, some difference is revealed on the leeward faces because the vortices in the gap become weaker and are formed far from the leeward faces, as shown in Figs. 12 and 13, after the addition of the central grids. In addition, a large fluctuating pressure on the bottom face of the upstream girder behind the overhaul track is observed because of the noticeable flow separation.

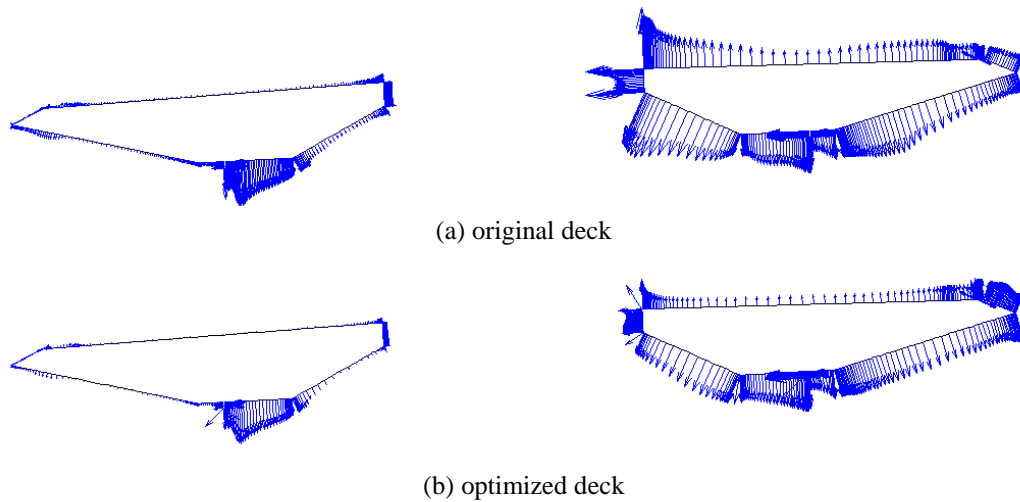


Fig. 15 The distribution of the fluctuating pressure on the surfaces

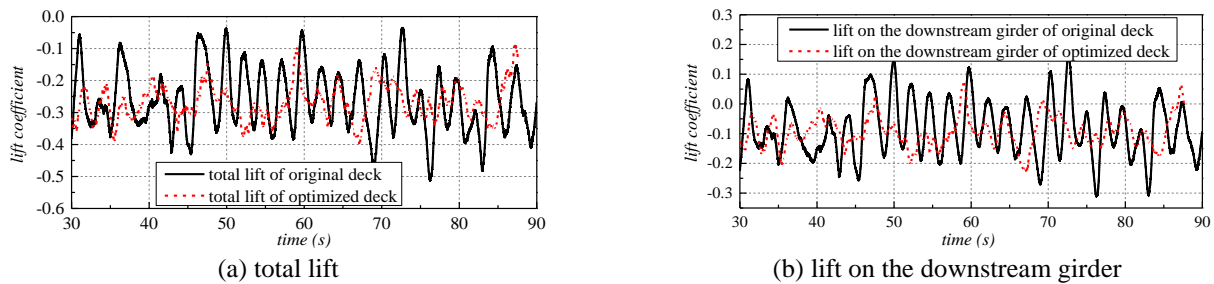


Fig. 16 Time histories of the total lift coefficients

Table 2 Mean and fluctuating lift coefficients

Cross section	Mean total lift	Mean lift on downstream girder	RMS of total lift	RMS lift on downstream girder
Original deck	-0.255	-0.089	0.113	0.096
Optimized deck	-0.257	-0.093	0.055	0.050

In contrast, the downstream girders for the original and optimized decks show apparently different fluctuating pressure distributions, with the original deck showing a higher feature whereas the optimized deck shows a lower feature overall. As mentioned above, the vortices impinge alternately onto both the upper side and the lower side of the downstream girder in the case of the original deck, causing the higher fluctuating pressure on the top plate relative to that in the case of the optimized deck. Similarly, the fluctuating pressure on the facade and inclined plates of the original deck has a higher value than that of the optimized deck.

This result illustrates that the vortices in the central vent become weaker as a consequence of the presence of the central grids.

Fig. 16 presents the time history of the lift coefficients for the whole deck and the single downstream girder, where the red line represents the lift coefficients of the optimized deck, and the black line represents those of the original deck. The lift coefficient time history is characterized by the oscillating frequency and the magnitude of maximum lift coefficients. As shown in Fig. 16, the dominant frequency of the total lift coefficients, as well as the mean lift coefficients, is nearly the same with and without the central grids. However, the total lift fluctuation (RMS value of lift coefficients) on the original deck is 0.113, which is significantly higher than the value of 0.055 of the optimized deck, as shown in Table 2. Similarly, the lift fluctuation on the downstream girder is also suppressed and decreases from 0.096 to 0.050 because the vortices that impinge onto

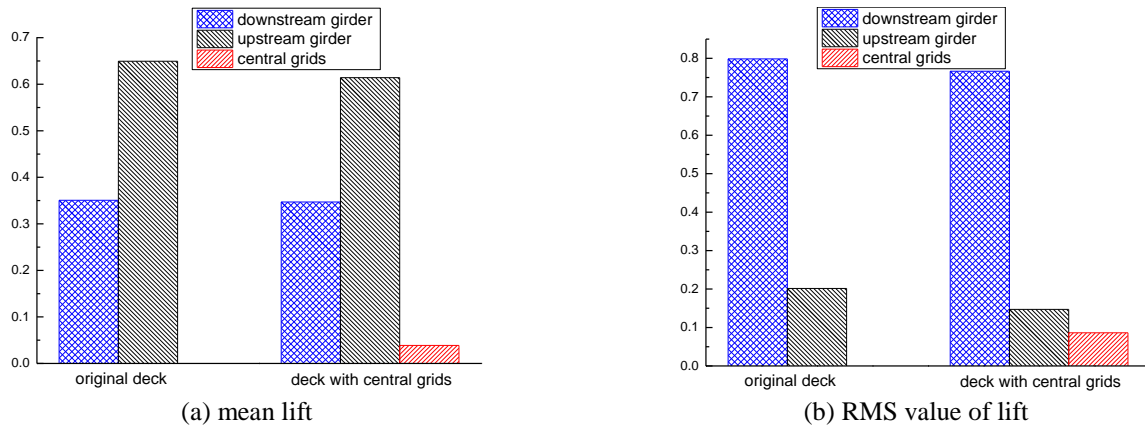


Fig. 17 Components of the mean and fluctuating lift forces

the downstream girder are suppressed by the existence of the central grids and become weaker, as mentioned above.

It can also be observed that the presence of the central grids suppresses the magnitude of the fluctuating lift coefficient without influencing the frequency of vortex shedding.

In addition, we analyzed the components of the mean and fluctuating lift forces to provide further understanding of the suppression effect caused by the central grids and the characteristics of the aerodynamic forces, as shown in Fig. 17. Whether considering the original deck or the optimized deck, the contribution of the mean lift on the downstream to the total lift is greater than 62 because the first vortex exists behind the trailing oblique webs of the upstream girder. Regarding the fluctuating lift, the total fluctuating lift is mainly provided by the downstream girder, accounting for nearly 80%. This result suggests that the mean total lift is mainly contributed by the upstream girder, whereas the fluctuating lift is mainly contributed by the downstream girder. This phenomenon was also found in the case of staggered cylinders (Sumner 2010, Zhou and Alam 2016). Notably, both the mean and fluctuating lifts on the central grids are less than 10% of the total mean and fluctuating lifts, respectively.

5. Conclusions

A numerical study based on a DDES was performed to investigate the flow over two twin box girders at a Reynolds number $Re=2.5 \times 10^4$, which is consistent with the experimental flow condition. The Strouhal number, drag, and lift moment coefficients, as well as the unsteady wake structures, were studied to enhance our understanding of the VIV performance and the suppression of VIVs by central grids. Several conclusions based on the study results are as follows:

- The flow, which is separated as it passes over the upper railings and the lower overhaul track of the upstream girder, induces large-scale vortices that impinge onto the downstream girder. A severe vertical VIV of the original two twin box girders

induces an evident lift fluctuation on the downstream girder as a result of the impingement of large-scale vortices.

- The fluctuating pressure on the facade and inclined plates of the downstream girder is obviously reduced by placing central grids in the gap because the strength of the vortices in the central gap, as well as their interaction, becomes weaker. Thus, a slightly fluctuating lift force was found on the optimized deck, and the vertical VIV is apparently suppressed.
- The mean total lift is mainly caused by the upstream girder, whereas the fluctuating total lift is mainly caused by the downstream girder.

Acknowledgments

This research was funded in part by the Natural Science Foundation of China (NSFC, No. 51378442 and 51708462) and the Fundamental Research Funds for the Central Universities (No.2682016CX006).

References

- Alam, M.M., Moriya, M., Takai, K. and Sakamoto, H. (2003), "Fluctuating fluid forces acting on two circular cylinders in a tandem arrangement at a subcritical Reynolds number", *J. Wind Eng. Ind. Aerod.*, **91**(1), 139-154.
- Chen, W.L., Li, H. and Hu, H. (2014), "An experimental study on the unsteady vortices and turbulent flow structures around twin-box-girder bridge deck models with different gap ratios", *J. Wind Eng. Ind. Aerod.*, **132**, 27-36.
- Chen, Z.Q., Niu, H.W. and Li, C.G. (2007), "Experimental study on wind-induced vortex shedding of parallel box-girder bridge", *J. Hunan University (Natural Sciences)*, 9 005.
- de Miranda, S., Patruno, L., Ricci, M. and Ubertini, F. (2015), "Numerical study of a twin box bridge deck with increasing gap ratio by using RANS and LES approaches", *Eng. Struct.*, **99**, 546-558.
- Ge, Y.J. and Xiang, H.F. (2008), "Bluff body aerodynamics application in challenging bridge span length", *Proceedings of 6th International Colloquium on Bluff Bodies Aerodynamics and*

Applications, July.

- Hua, X., Chen, Z., Chen, W., Niu, H. and Huang, Z. (2015), "Investigation on the effect of vibration frequency on vortex-induced vibrations by section model tests", *Wind Struct.*, **20**(2), 349-361.
- Hui, M.C., Ding, Q. and Xu, Y. (2006), "Flutter analysis of Stonecutters Bridge", *Wind Struct.*, **9**(2), 125-146.
- Kargarmoakhar, R., Chowdhury, A.G. and Irwin, P.A. (2015), "Reynolds number effects on twin box girder long span bridge aerodynamics", *Wind Struct.*, **20**(2), 327-347.
- Kwok, K.C., Qin, X.R., Fok, C. and Hitchcock, P.A. (2012), "Wind-induced pressures around a sectional twin-deck bridge model: Effects of gap-width on the aerodynamic forces and vortex shedding mechanisms", *J. Wind Eng. Ind. Aerod.*, **110**, 50-61.
- Larsen, A., Savage, M., Lafrenière, A., Hui, M.C. and Larsen, S.V. (2008), "Investigation of vortex response of a twin box bridge section at high and low Reynolds numbers", *J. Wind Eng. Ind. Aerod.*, **96**(6), 934-944.
- Leonard, B. (1991), "The ULTIMATE conservative difference scheme applied to unsteady one-dimensional advection", *Comput. Method. Appl. M.*, **88**(1), 17-74.
- Li, H., Laima, S., Ou, J., Zhao, X., Zhou, W., Yu, Y., Li, N. and Liu, Z. (2011), "Investigation of vortex-induced vibration of a suspension bridge with two separated steel box girders based on field measurements", *Eng. Struct.*, **33**(6), 1894-1907.
- Matsumoto, M., Shijo, R., Eguchi, A., Hikida, T., Tamaki, H. and Mizuno, K. (2004), "On the flutter characteristics of separated two box girders", *Wind struct.*, **7**(4), 281-291.
- Matsumoto, M., Yagi, T., Tamaki, H. and Tsubota, T. (2008), "Vortex-induced vibration and its effect on torsional flutter instability in the case of B/D= 4 rectangular cylinder", *J. Wind Eng. Ind. Aerod.*, **96**(6), 971-983.
- Menter, F., Kuntz, M. and Langtry, R. (2003), Ten years of experience with the SST turbulence model. *Turbulence Heat Mass Transfer 4*, 625-632, Begell House Inc
- Nieto, F., Kusano, I., Hernández, S. and Jurado, J. (2010). "CFD analysis of the vortex-shedding response of a twin-box deck cable-stayed bridge", *Proceedings of the 5th International Symposium on Computational Wind Engineering*, Chapel Hill, NC.
- Ogawa, K., Shimodoi, H. and Oryu, T. (2002), "Aerodynamic characteristics of a 2-box girder section adaptable for a super-long span suspension bridge", *J. Wind Eng. Ind. Aerod.*, **90**(12), 2033-2043.
- Patankar, S.V. and Spalding, D.B. (1972), "A calculation procedure for heat, mass and momentum transfer in three-dimensional parabolic flows", *Int. J. Heat Mass Tran.*, **15**(10), 1787-1806.
- Sohankar, A. (2008), "Large eddy simulation of flow past rectangular-section cylinders: Side ratio effects", *J. Wind Eng. Ind. Aerod.*, **96**(5), 640-655.
- Spalart, P., Jou, W., Strelets, M. and Allmaras, S. (1997), "Comments on the feasibility of LES for wings, and on a hybrid RANS/LES approach", *Advances in DNS/LES*. 1 4-8.
- Spalart, P.R., Deck, S., Shur, M., Squires, K., Strelets, M.K. and Travin, A. (2006), "A new version of detached-eddy simulation, resistant to ambiguous grid densities", *Theor. Comput. Fluid Dynam.*, **20**(3), 181-195.
- Sumner, D. (2010), "Two circular cylinders in cross-flow: a review", *J. Fluid. Struct.*, **26**(6), 849-899.
- Sun, D., Owen, J.S., Wright, N.G. and Liaw, K.F. (2008), "Fluid-structure interaction of prismatic line-like structures, using LES and block-iterative coupling", *J. Wind Eng. Ind. Aerod.*, **96**(6), 840-858.
- Trein, C.A., Shirato, H. and Matsumoto, M. (2015), "On the effects of the gap on the unsteady pressure characteristics of two-box bridge girders", *Eng. Struct.*, **82**, 121-133.
- Xu, K., Ge, Y. and Zhang, D. (2015), "Wake oscillator model for assessment of vortex-induced vibration of flexible structures under wind action", *J. Wind Eng. Ind. Aerod.*, **136**, 192-200.
- Xu, K., Ge, Y., Zhao, L. and Du, X. (2017), "Experimental and numerical study on the dynamic stability of vortex-induced vibration of bridge decks", *Int. J. Struct. Stab. Dynam.*, 1850033.
- Yang, Y. and Ge, Y. (2009), "Aerodynamic flutter control for typical girder sections of long-span cable-supported bridges", *Wind Struct.*, **12**(3), 205-217.
- Yang, Y., Zhou, R., Ge, Y. and Zhang, L. (2016), "Experimental studies on VIV performance and countermeasures for twin-box girder bridges with various slot width ratios", *J. Fluid. Struct.*, **66**, 476-489.
- Zhou, Y. and Alam, M.M. (2016), "Wake of two interacting circular cylinders: A review", *Int. J. Heat Fluid Fl.*, **62**, 510-537.
- Zhou, Z. and Ma, R. (2010), "Numerical simulation study of the Reynolds number effect on two bridge decks based on the deterministic vortex method", *Wind Struct.*, **13**(4), 347-362.
- Zhou, Z., Yang, T., Ding, Q. and Ge, Y. (2015), "Mechanism on suppression in vortex-induced vibration of bridge deck with long projecting slab with countermeasures", *Wind Struct.*, **20**(5), 643-660.